Talanta 85 (2011) 927–935

Contents lists available at ScienceDirect

Talanta

journal homepage: www.elsevier.com/locate/talanta

Electrochemical impedance spectroscopy as a highly sensitive tool for a dynamic interaction study between heparin and antithrombin: A novel antithrombin sensor

S. Haddad [a,b], S.M. Derkaoui [b], T. Avramoglou [b], E. Ait [c], A. Othmane [a], L. Mora [b,*]

[a] Biophysics Laboratory, Faculty of Medicine of Monastir, 5019 Monastir, Tunisia
[b] INSERM U 698 Laboratoire de Bio-Ingénierie de Polymères Cardiovasculaires, Université Paris 13, 99 av JB Clément, Institut Galilée, 93430 Villetaneuse, France
[c] UPR 3407 Laboratoire des Sciences des Procédés et des Matériaux, Université Paris 13, 99 av JB Clément, Institut Galilée, 93430 Villetaneuse, France

ARTICLE INFO

Article history:
Received 13 October 2010
Received in revised form 21 April 2011
Accepted 29 April 2011
Available online 11 May 2011

Keywords:
Heparin
Antithrombin
Polybutyl methacrylate
SS316L
EIS

ABSTRACT

Specific recognition between two biological partners is widely exploited in biosensors nowadays. To explore this avenue, a novel biosensor for antithrombin (AT) detection was constructed. Heparin was used as the affinity ligand.

A well-known acrylic monomer (butyl methacrylate) was polymerized and grafted onto the heparin polysaccharide by the use of ceric ammonium nitrate as a redox initiator in aqueous nitric acid medium. Polymers were deposited as a thin layer onto surface of stainless steel electrode (SS316L).

The obtained polymers were studied by Fourier transform infrared spectroscopy (FTIR) and analyzed by differential scanning calorimetry (DSC).

Moreover, the films were characterized by electrochemical impedance spectroscopy (EIS), contact-angle measurements and AFM.

EIS was used to study the biosensor affinity to AT and the relationship between functionalization growth of modified electrode and the response of the sensor.

The proposed approach appears to be simple, sensitive and correlated with methods that analyse the detection of antithrombin.

1. Introduction

Different varieties of heparin are widely used for surface modifications of biomaterials [1] in order to prevent activation of coagulation, of complement system and inflammatory reactions due to the exposure of artificial biomaterials to blood in the human body [2]. Heparin, a natural component in the human body, is a well-known and efficient anticoagulant due to its ability to accelerate the inhibitory effect of antithrombin (AT) [3–5].

When bound to heparin species, AT undergoes a conformational change, whereby the rate of inactivation of a broad range of coagulation factors is greatly accelerated [6]. Heparin, if properly attached to a surface, may retain its capacity to down-regulate the enzymatic coagulation mechanism, minimize the adhesion and activation of platelets and white blood cells, and, moreover, decrease the complement activation [7–12].

It has been suggested that immobilizing heparin on a surface would be more effective as compared to delivery in solution because it would improve biological performance locally due to the local capacity for antithrombin (AT) binding. However, the immobilization of heparin onto a solid surface must be in such a manner as to facilitate the uptake of AT and the subsequent complex formation. Many studies of heparin immobilized onto a variety of polymer surfaces, such as polyurethane, polydimethylsiloxane [13], polyvinylidene fluoride [14], poly(L-lactic acid) [15], polyethylene [16], and polytetrafluoroethylene [17] have been reported to significantly increase the biocompatibility of the materials. In biomaterial research, ATH covalent complexes of antithrombin (AT) and heparin (H) based surface coatings can be used to improve the biocompatibility of metallic surfaces such as vascular stents. The disadvantage of the covalently coated heparin surface is that the heparin has low bioactivity [18]. Thus, although a number of studies [19,20] have demonstrated some utility in heparin coating of vascular catheters for thrombosis inhibition, long-term biocompatibility of heparinized surfaces in vivo may be limited [21,22].

Various methods have been used in the study of heparin–protein interactions including affinity chromatography, SPR, nuclear magnetic resonance (NMR), fluorescence spectroscopy, affinity coelectrophoresis, two-dimensional affinity resolution electrophoresis, equilibrium dialysis, competitive binding techniques, analytical

* Corresponding author. Tel.: +33 01 49 40 36 63; fax: +33 01 49 40 30 08.
E-mail address: Laurence.mora@univ-paris13.fr (L. Mora).

0039-9140/$ – see front matter © 2011 Elsevier B.V. All rights reserved.
doi:10.1016/j.talanta.2011.04.079

centrifugation, and circular dichroism [23]. A home-made quartz crystal microbalance-flow injection analysis (QCM-FIA) system with data analysis software developed by a Chinese group was used to determine the interaction between immobilized heparin and AT. A linear poly(glycidyl methacrylate) (PGMA) with epoxy groups was used as a coating material covering the surface of an electrode area of a QCM device that allowed easy coupling of heparin molecules onto the electrode and thus facilitated the determination of the dynamic interaction between heparin and AT. This method allowed for the quick determination of the kinetic parameters between two biomolecules [24]. Recently, a novel biosensor for detecting AT was constructed based on *in situ* growth of nanogold on the gold electrode of QCM. Heparin wad used as the affinity ligand and immobilized onto the nanogold modified gold electrode [25]. Although QCM sensors have been proved to be versatile in various applications, the sensor response still needs to be improved for detecting the expensive or low-content-biological samples [25].

In the present investigation, an attempt has been made to construct a new kind of biosensor by immobilization of heparin onto the surface of the biomaterial. The interaction between heparin and antithrombin was evaluated by electrochemical impedance spectroscopy (EIS).

EIS has been extensively exploited for the characterization of materials and surface modification procedures, and well as for monitoring of binding events. The fact that impedance measurements can be performed in a reagent makes it very attractive for biosensors development [26,27]. The equipment required is compact, does not contain mobile parts, and is easy to miniaturise, suggesting that EIS biosensors could be easily used in-field with minimal requirements. Furthermore, impedance combines rapid response, low detection limits, cost-effectiveness, and the possibility of performing real-time monitoring.

Biocompatibility of copolymers was also evaluated (data not shown) [28].

2. Materials and methods

2.1. Materials

Heparin and antithrombin were purchased from Aldrich. Butyl methacrylate monomers were obtained from Acros France and were purified by washing with 5% NaOH and 20% NaCl, followed by distilled water. Ammonium cerium (IV) nitrate (Acros France) was dried at 80 °C under vacuum for 24 h. Solvents were of the highest commercially available purity.

2.1.1. Graft copolymerization of the acrylic monomers

Heparin was dissolved in 500 mL of nitric acid (0.2 M), and the reactor was placed in an oil bath at 40 °C. After the complete dissolution of the polysaccharide to form a homogeneous solution (10 min), 5 ml of solution of Ce(IV) (2.4×10^{-4} mol/l) and 2 ml of butyl methacrylate were simultaneously added to the reaction mixture, and after 40 min, the reaction product was allowed to cool at ambient temperature. The mixture was raised to pH 8 by the addition of NaOH aqueous solution (10 M), and it was concentrated with a Heidolph rotary evaporator. Then, the product was precipitated in 200 mL of methanol. The particle suspensions were dialyzed against permanently renewed tap water for 48 h and were washed twice with 50 mL of EDTA (10^{-2} M), followed by three washes with 50 mL of distilled water to remove cerium ions and the heparin that did not react. The purified copolymer was frozen at −20 °C and lyophilized for 24 h. Homopolymer was extracted with acetone. Pure copolymer was dried under vacuum and was weighed. The obtained copolymer was named heparin graft poly(butyl methacrylate) and will be noted: PBMA-Hep.

2.1.2. SS 316L substrate preparation before film deposition

SS 316L plates (Ø of 12.7 mm and thickness of 2 mm) were obtained from Good fellow industries (Devon, PA, USA). SS 316L plates were used for contact angle and EIS measurements of the modified surfaces. The pre-treatment of the metal substrate surfaces is very important for obtaining uniform coatings.

The SS 316L was mechanically polished and cleaned in an ultrasonic cleaner with acetone for 15 min, then with ethanol. Finally, SS 316L substrates were rinsed with distilled water three times and immediately dipped in a methanol solution.

2.1.3. Preparation of films

A large number of films have been prepared and used for various physicochemical characterizations.

Films were prepared using 15 mg of dried homopolymer PBMA solubilized in THF. Copolymer PBMA-Hep was dissolved in 1 ml of THF/H_2O (92:8) treated in ultrasonic bath for 1 h. To obtain films, solutions were deposited as a thin layer on the cleaned SS 316L substrates at room temperature for 24 h in saturated atmosphere of THF and in the presence of $CaCl_2$ to absorb water. The samples were dried for 24 h to remove the remaining solvent.

Films adhere on the SS 316L electrodes by physical adsorption. Samples thus prepared were rinsed several times with phosphate buffer solution (PBS, pH 7.4) before utilization. The polymeric film thickness has been estimated using a micrometer to about 35 μm.

2.2. Characterizations

2.2.1. Infrared spectral analysis

The infrared spectra of heparin, PBMA, and copolymer PBMA-Hep were obtained from a Perkin-Elmer 1600 spectrometer. Dried samples (1.5 mg) were ground with KBr powder (150 mg) and were pressed into pellets for FT-IR examination. Omnic software was used for data acquisition and analysis.

2.2.2. Differential scanning calorimetry (DSC)

The thermal behavior of polymers (heparin, PBMA, PBMA-Hep) was analyzed with a Setaram DSC131 thermal analyzer operating in combination with the liquid nitrogen cooling accessory. The furnaces were purged with nitrogen, and samples were passed in a temperature range of 0–200 °C at a heating rate of 10 °C/min. In each case, two consecutive scans were carried out on each sample. The glass transition temperature (T_g) of the polymers was taken as the midpoint in the shift of the heat flow baseline.

2.2.3. Contact angle

For an evaluation of surface wettability, the water contact angles of films were measured at room temperature using a contact angle measurement system (Krüs, model DSA 10-MK2). A droplet of deionized water (2 μl) was put on the air-side surface of the films and the contact angle was measured. The process was monitored by a video camera.

Measurements were repeated three times for each sample. Each type of surface modification was studied in duplicate, and the average of all six measurements was calculated and reported.

2.2.4. Atomic force microscopy (AFM)

In addition to the surface chemical composition, surface roughness also plays a very important role in determining the wettability of a film [29,30]. Tapping mode AFM with topographical detection was used to observe the nanoscale surface roughness of the films [31].

Surface topography of the films was characterized by atomic force microscopy (AFM) under ambient conditions, using a Nanoscope III equipped with a scanner 1553 D (Digital Instruments, Santa Barbara, CA, USA). All AFM images were taken by means of

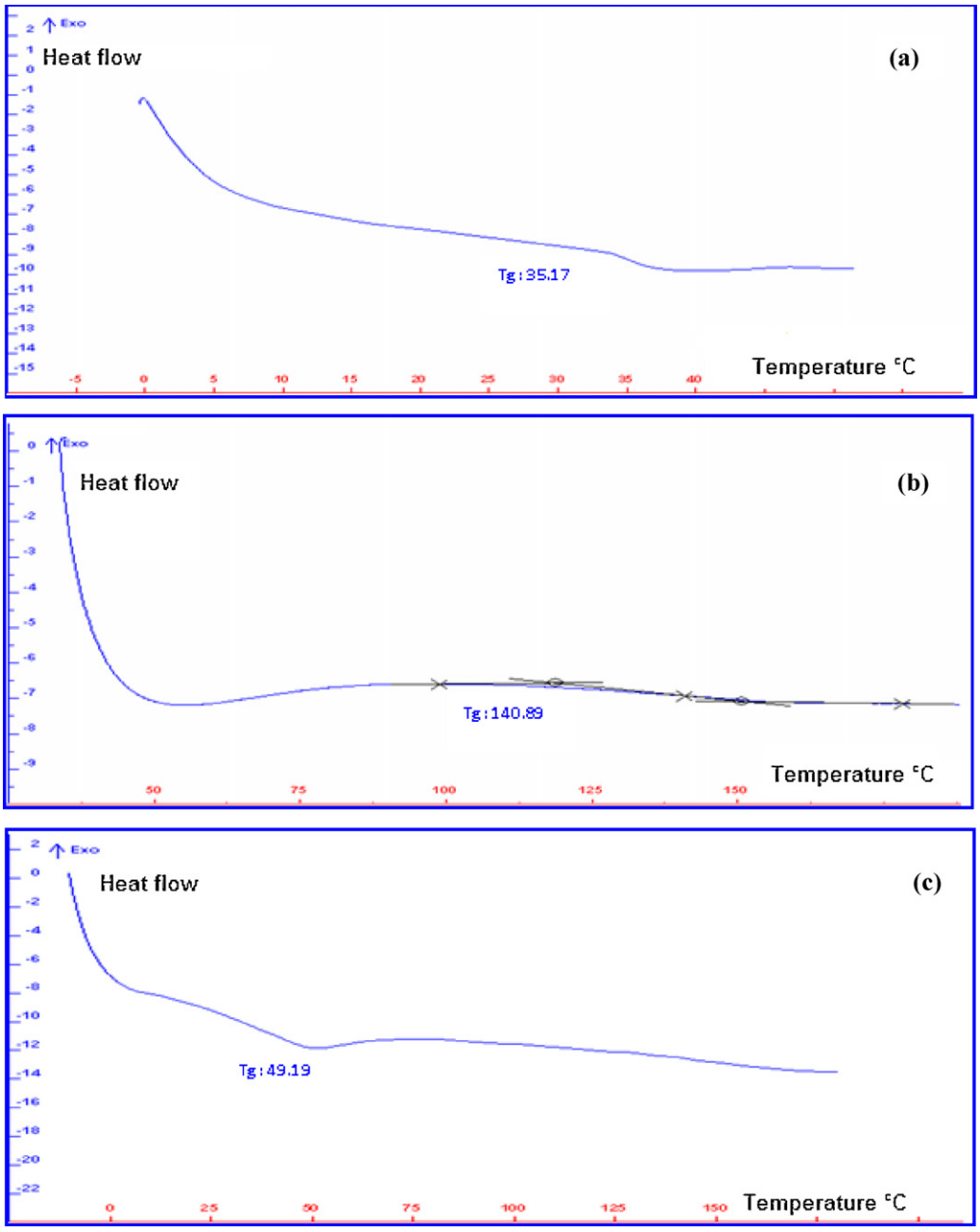

Fig. 1. DSC thermograms of: (a) PBMA, (b) heparin and (c) copolymer PBMA-Hep. In each case, two consecutive scans were carried out on each sample. The T_g was as the mid-point in the shift of heat flow baseline.

tapping mode. All the AFM images were made in air at room temperature. The surface feature size and roughness parameters were therefore determined by the AFM software program.

2.2.5. Electrochemical measurements

A conventional three electrode cell was used for all the electrochemical measurements. A saturated calomel electrode (SCE) was used as a reference electrode, platinum foil was the counter electrode and the test material was taking as the working electrode. The impedance analysis was performed with a Voltalab PGZ301 analyser.

EIS was performed in the frequency range 10 mHz to 100 kHz. During measurements the potential was kept at −290 mV as non corrosive potential. The alternative potential applied to the working electrode was of 10 mV s^{-1}.

All electrochemical measurements were carried out at room temperature in a Faraday cage and were performed in PBS (Phosphate Buffer solution) pH 7.4. Each electrochemical measurement was repeated at least three times. The Zview modelling program (Scribrer and Associates, Charlottesville, VA) was used to analyse impedance data.

All EIS measurements were made on different types of polymers. Obviously for each measurement we use one film (of each type), for concentration studies, we obtained Nyquists with a single electrode, starting from low to higher concentrations.

2.2.6. Statistical analysis

Contact angle measurements were treated with an Excel software version Microsoft 2007. The Student's statistical test was used for comparisons of the different surfaces. Probabilities of correla-

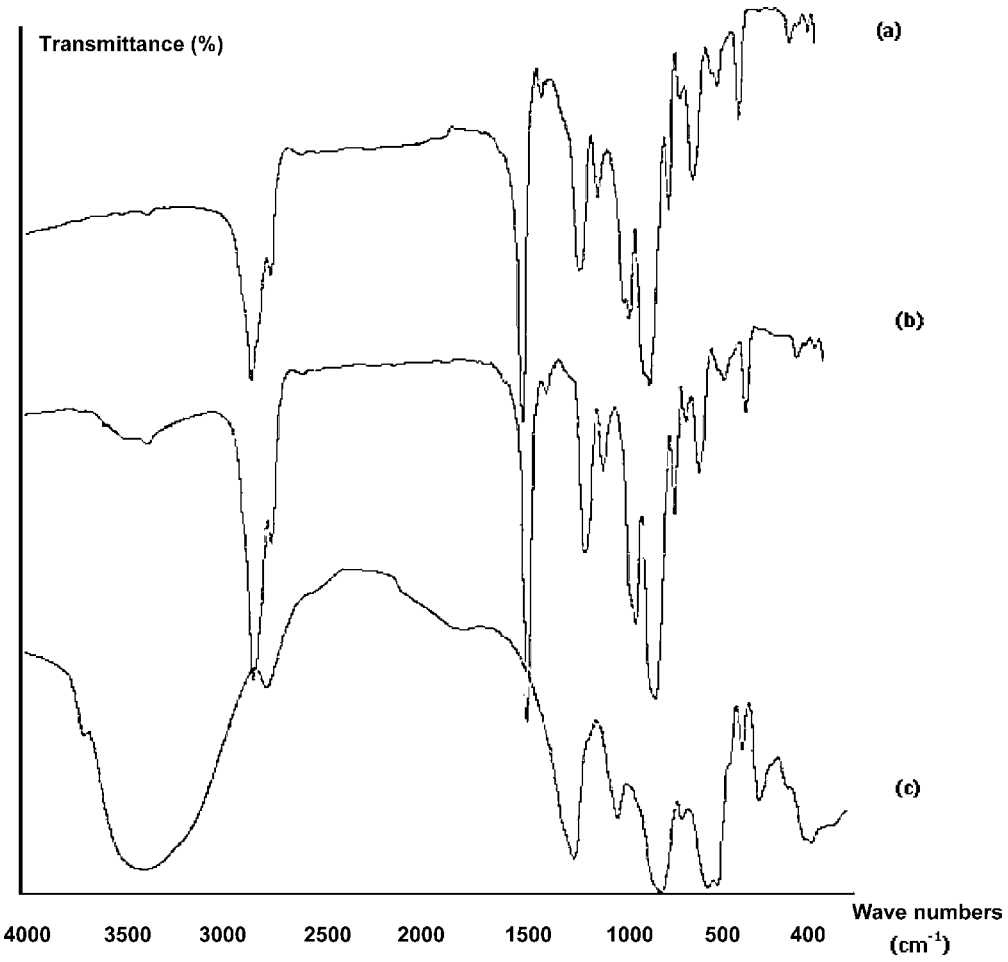

Fig. 2. Fourier transforms infra-red spectra of (a) PBMA, (b) PBMA-Hep and (c) heparin. Note the presence of typical absorption band of PBMA at 1730 cm^{-1} corresponding to C=O stretching vibrations, and characteristic band for heparin.

tion using the Pearson's coefficient (p) considered correct p values below 0.05 as a statistically significant threshold.

3. Results and discussion

3.1. Differential scanning calorimetry (DSC)

The determination of the glass-transition temperature was carried out for heparin, PBMA, and copolymer PBMA-Hep (Fig. 1). The T_g values of the two homopolymers PBMA (Fig. 1a) and heparin (Fig. 1b) were 35.17 and 140.89 °C, respectively. A single T_g was obtained at 49.19 °C for copolymer PBMA-Hep (Fig. 1c). This value is thus intermediate as compared with the homopolymers.

It is well known that in the DSC analysis of polymer binary mixtures, detection of a single glass transition (T_g), whose temperature is intermediate between those corresponding to the two component polymers, is the most unambiguous criterion of polymer miscibility [32].

3.2. Fourier transforms infrared spectroscopy studies

As shown in Fig. 2, spectra showed the presence of typical absorption band of PBMA at 1726.68 cm^{-1} (Fig. 2a) corresponding to C=O stretching vibrations. The IR spectrum obtained for heparin alone (Fig. 2c) showed bands of main functional groups in the disaccharide units (COO^-, SO_3^-, OH, NH and C–O–C). These bands around 1600 and 1000 cm^{-1} correspond to stretching vibrations of the carboxylate and ether groups [33].

The spectrum of PBMA-heparin film (Fig. 2b) shows an increase in peak intensities around 2959.98 and 966.16. Furthermore, the existence of heparin is proved by the peak at 3433.70 cm^{-1}, which could be assigned to the hydroxyl stretching vibrations of heparin molecule. The peak at 1269 cm^{-1} can be attributed to the symmetric stretching vibration and asymmetric vibration of $-SO_3$ units of heparin.

These results proved the presence of heparin and butylmethacrylate simultaneously on the film coating substrates.

3.3. Water contact-angle analysis

The contact angle measurement method is probably the most definitive way to determine the hydrophobicity of material surfaces. The angle is very high for water if the substrate is hydrophobic. When the surface is hydrophilic, the droplet quickly dissipates and the measured angle is low. Like other methods, the contact angle method gives an average value for hydrophobicity [34]. Contact angles change with surface topography, surface tension of the liquid, surface energy of the substrate, and level of interaction between the liquid and solid [35–37].

The water contact-angle value measured on SS 316L was $60.2 \pm 1.6°$. Contact angle measurements, performed using PBMA and PBMA-Hep plates, produced typical values of 89.22 ± 2.7 and $82.42 \pm 1.6°$ respectively. Heparin immobilization is expected to increase the wettability of the surface, as reported earlier in the literature [38]. The heparin molecule contains numerous hydrophilic

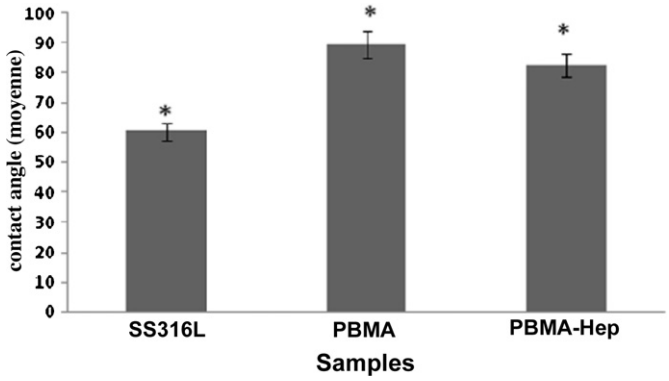

Fig. 3. Contact angle measurements.

groups such as –OH, –O–, R–COO$^-$, R–O–SO_3^- and R–NH–SO_3^- that are free to hydrogen bond to water molecules.

Values of water contact-angle measured on SS 316L, PBMA and PBMA-Hep covered plates, seem close but through student testing it was found that the difference is statistically significant ($p < 0.05$) (Fig. 3). The p values are 8.59E−8, 3.03E−8 and 0.001 for SS 316L vs PBMA, SS 316L vs PBMA-Hep and PBMA vs PBMA-Hep respectively.

3.4. Morphology of film coating on SS 316L by AFM

Films could be imaged by an atomic force microscope (AFM) and characterized by roughness rate (the root mean square: RMS) as a scale for surface roughness. Fig. 4 shows the AFM line profile of the surface of the PBMA (Fig. 4a) and PBMA-Hep (Fig. 4b) films. The variation of roughness rate proves that the monomer (butyl methacrylate) was successfully grafted onto the polysaccharide heparin (R_a = 9.73 nm vs 6.88 nm for PBMA-Hep and PBMA respectively). The line profile of the AFM images suggests that the roughness of PBMA is lower than that of PBMA-Hep due to the presence of heparin onto PBMA.

It seems there is no distinct relationship between hydrophilicity and roughness of PBMA ad PBM-Hep films. Chemical composition affects more the film wettability than surface morphology [29].

3.5. EIS analysis of SS316L with and without polymer film

The modified and unmodified electrodes were tested and subjected to reproducibility. All measurements were repeated three times for each sample (coated and uncoated samples) to confirm that the measurements are reproducible and stable.

The obtained electrode coating was chemically stable during the measurement and retains the biological activity for target samples.

Before acquiring the impedance spectra, the open circuit potentials of the different electrodes were measured until potential stabilization was achieved, which occurred after 10–15 min of immersion.

The electrical properties of PBMA and PBMA-Hep films were examined by EIS. The impedance spectra are generally determined by both the charge transfer at the electrolyte/electrode interface and the mass transport in the solution.

Typical Nyquist diagrams of the SS 316L coated and uncoated bare electrodes are shown in Fig. 5. The impedance-plane plots of non functionalized (bare 316L) electrode and PBMA coated electrode are characterized by two semicircles. The first one appeared probably due to the resistance of the thin oxidative layer. On exposure to air an oxide layer is formed spontaneously on the surface of biomedical alloys [39,40].

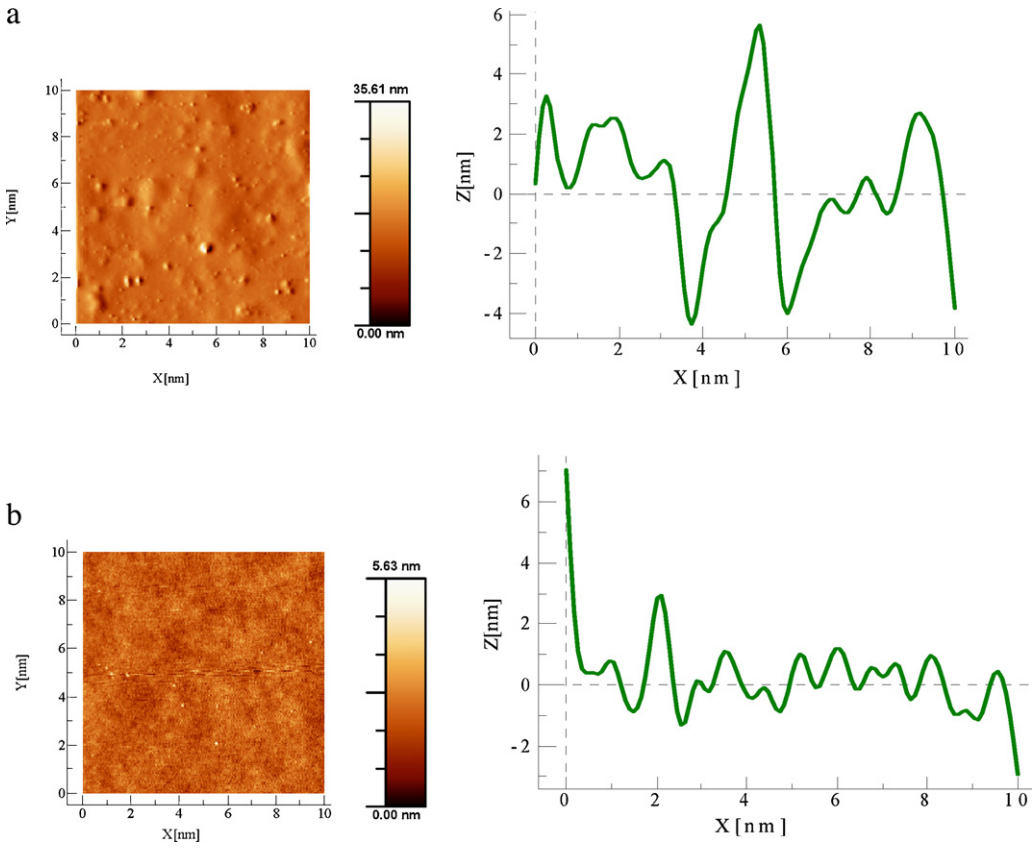

Fig. 4. AFM topography images and profiles: (a) PBMA topography functionalized SS 316L electrode; (b) PBMA-heparin topography functionalized SS 316L electrode.

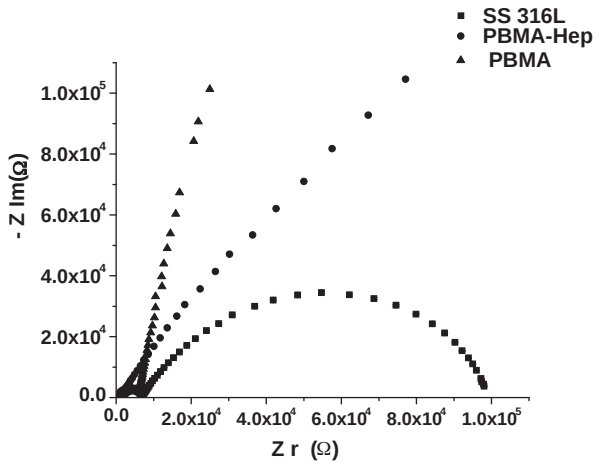

Fig. 5. Nyquist diagrams (Zr vs Zi) and bodes for the impedance measurements corresponding to SS 316L electrode, PBMA coated electrode and PBMA-Hep coated electrode. All measurements were performed in PBS pH 7.4. Amplitude of alternating voltage is 10 mV. Symbols show the experimental data in PBS solution.

On the other hand, the inorganic ions such as HPO_4^{2-} and $H_2PO_4^{2-}$, that are present in PBS solution, could be adsorbed on the stainless steel and should form an ion layer [41].

Qinggang et al. [42] showed that the impedance spectra of the bare 316L stainless steel, exhibit a small semicircle line probably due to the resistance of the thin oxidative layer.

The Nyquists of PBMA-Hep and PBMA coated SS 316 L substrate were appreciably different from that of the uncoated stainless steel substrate. It is possible that the films coating acts as an active site blocker and thus reducing the effective electro active area.

The studied polymers present different interfacial characteristics. The curve of PBMA-Hep assumes a more resistive semi circular profile for the film impedance.

PBMA and PBMA-Hep do not have the same properties, for this reason we do not see the first semi circle for PBMA-Hep like for PBMA. This trend can be related to the morphology of porosity in films, higher irregularities and breakdown of PBMA films. Certainly, polymer breakdown due to the formation of pores would give rise to significant differences in the impedance spectra.

For PBMA (Fig. 5), a small capacitive semicircle, followed by an incomplete capacitance arc was observed. The first is related to charge transfer resistance (R_{ct}) for processes occurring at the bottom of the pores of the coating. C_{dl} is the double layer capacitance which is due to charge separation at metal/electrolyte interfaces. The second one at the middle and low frequency region is attributed to the sum of porous oxide and polymer film resistances (R_f). C_f can be defined as parallel capacitances which were built up from ion exchange for charge compensation at the polymer/electrolyte interface and from ion diffusion through the pores of the coatings at the metal/polymer interface [43,44].

To prove that the straight line is not corresponding to diffusion for PBMA film, we plotted the curve $\log_{10}(-Z_i)$ vs $\log_{10}$(frequency) and we calculated the slope:

- If slope = −0.5, it is a diffusion.
- If the value is close to 0.8–1, there is a beginning of second semicircle with increased R_{ct}.

We have thus found a value of 0.74. This value is close to 0.8, and then we justified our hypothesis [45].

Impedance spectra may be interpreted through equivalent circuits representing the different processes involved in the description of the system with discrete electric elements.

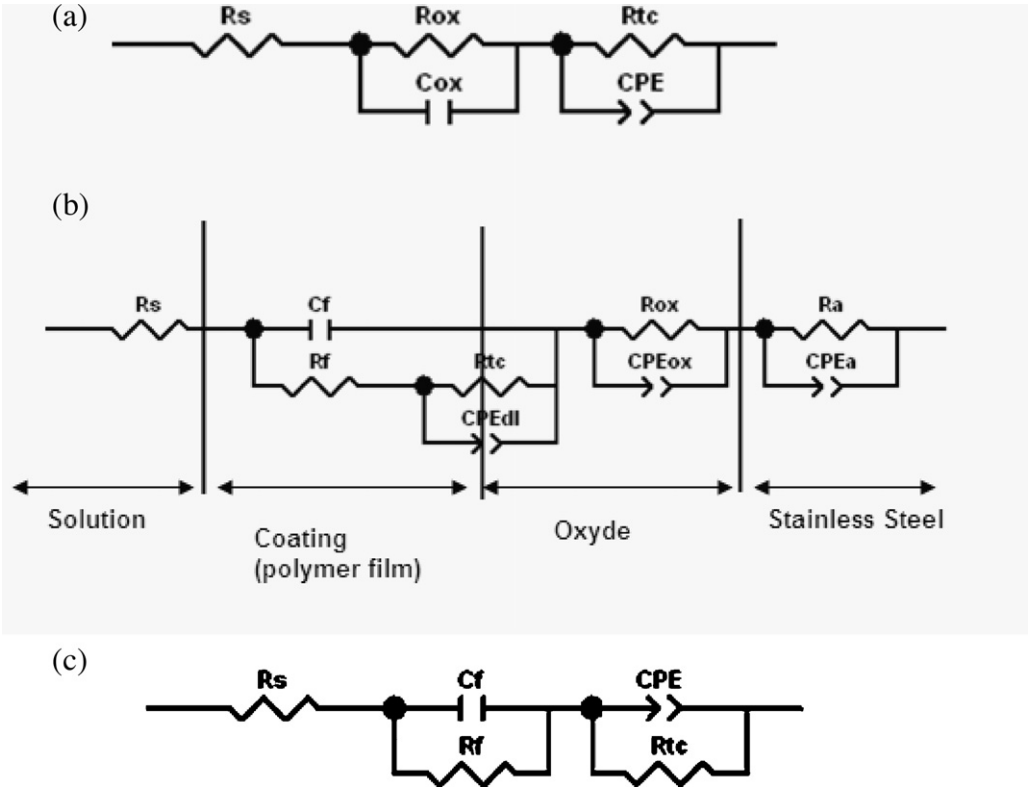

Fig. 6. Equivalent circuit models used in this study: a represents the circuit for the bare SS 316L electrode; B and C have been used to model the modified electrodes; where R_s is the solution resistance, R_{ox} is the resistance of the oxide film, CPE_{ox} is the constant phase angle element of the oxide film, R_f is the film ohmic resistance, R_{ct} is the charge-transfer resistance, R_a is the resistance of SS 316L, CPE_a is the constant phase element of SS316L.

Table 1
Fitting values of the equivalent circuit elements of PBMA coated SS 316L electrode under various AT concentrations.

[AT] (U/ml)	R_s	C_f	R_f	*Rtc*	χ^2
PBMA*	326.7	5.42E−8	713,900	1.49E7	5.35E−4
0.05	300.4	4.93E−8	42,150	8.59E6	5.04E−4
0.1	337	4.47E−8	202,280	5.07E6	4.85E−4
0.15	324.1	4.16E−8	88,091	1.27E7	4.51E−4
0.2	320.5	4.15E−8	65,024	1.45E7	5.50E−4
0.25	311	4.02E−8	71,055	1.85E7	4.25E−4

* Films before making additions of AT.

Several electrical circuits were initially tested by fitting of the experimental impedance data.

The qualities of the fitting and the possibility to assign a physical meaning to the components have led the authors to propose the circuits in Fig. 6. The equivalent circuits were found to give excellent fits down to frequencies including the low frequency bulk capacitance of the polymer film.

The diameter of the semicircle provides an estimate of the film charge transfer resistance.

The equivalent circuits (Fig. 6) includes the ohmic resistance of the electrolyte solution (R_s); the film ohmic resistance (R_f); the resistance of the passivating film (R_{ox}); the interfacial charge-transfer resistance (R_{ct}), corresponding to the charge-transfer process; the constant phase element impedance (CPE_{dl}) being introduced in the circuit instead of the double layer capacitance because it reflects inhomogeneities and defect areas of the electrode surface [46].

The equivalent circuit presented in Fig. 6b is generally recognised as being representative of a deteriorating polymer-coated metal system [47] and has been used for data analysis throughout this paper.

The experimental impedance spectra of SS 316L and polymer coatings are fitted with a different equivalent electronic circuit (Fig. 6a for SS 316L, Fig. 6b for PBMA and Fig. 6c for PBMA-Hep), in order to analyse the electrochemical property of the two different films in details. The values of R_{ct} were extracted from the computer simulated spectra.

The different circuit models give a satisfactory fitting of the curves. The resistance of studied interface increases after immobilization of each step. This increase is due to the decrease of the conductivity due to the insulating properties of deposited polymeric films.

The lower R_{ct} value for the uncoated SS 316L, approximately $9.75 \times 10^4\ \Omega$, indicates that the ions present in the electrolyte can attack on the surface and this is attributed to the thinning of the passive film. The assembly of the PBMA monolayer film onto the electrode surface led to a further increase in the R_{ct} value ($1.49 \times 10^7\ \Omega$) (Table 1). We might expect an increase in the semicircle at high frequencies where the heterogeneous R_{ct} must increase due to the inhibition of the electron transfer rate. The increase in the R_{ct} is related to the electrode coverage.

The R_{ct} of the film with heparin (PBMA-Hep) increases to $5.64 \times 10^7\ \Omega$ (Table 2) due to the repulsion between the negatively charged interface and the negatively charged presents in the electrolyte. At physiological pH values, the main functional groups of heparin contain sulfate ($-OSO_3^-$, $-NHSO_3^-$) and carboxylate ($-COO^-$) groups that lead to a highly negatively charged molecule.

The CPE value extracted from the computer fitting for the PBMA and PBMA-Hep were 2.09 and 4.82 μF respectively.

To confirm the feasibility of the above preparation and assay of AT sensor, EIS was adopted to investigate specific adsorption of AT assay onto heparin. Impedance spectroscopy is a highly effective tool of probing the features of surface-modified electrodes [48,49].

Table 2
Fitting values of the equivalent circuit elements of PBMA-Hep coated SS 316L electrode under various AT concentrations.

[AT] (U/ml)	R_s	R_f	C_f	*Rtc*	χ^2
PBMA-Hep*	228.5	1.24E5	1.28E−5	5.64E7	1.01E−2
0.05	187.2	5.23E5	1.67E−5	2.08E12	5.60E−3
0.1	129.5	1.11E6	1.59E−5	5.60E12	2.10E−3
0.15	129.3	1.37E6	1.48E−5	7.93E12	2.43E−3
0.2	130.8	1.32E6	1.45E−5	6.34E16	2.40E−3
0.25	129.8	1.40E6	1.51E−5	3.34E17	2.41E−3
0.3	120.4	1.46E6	3.48E−7	3.35E17	2.21E−3
0.35	117.7	1.56E6	3.25E−7	3.37E17	2.38E−3
0.4	118.4	1.38E6	1.85E−7	3.39E17	2.30E−3
0.45	119.7	1.36E6	2.18E−8	3.55E17	2.00E−3
0.5	118.6	1.31E6	1.87E−8	3.60E17	2.30E−3
0.55	119.21	1.32E6	1.21E−8	5.70E17	2.71E−3
0.6	119	1.30E6	1.01E−8	7.98E17	2.52E−3
0.65	119.01	1.35E6	0.53E−8	9.01E17	2.31E−3

* Films before making additions of AT.

3.6. EIS analysis for antithrombin immobilization assay on functionalized electrode

When a target biomolecule interacts with a probe-functionalized surface, changes in the electrical properties of the surface (e.g., dielectric constant, resistance) can result solely from the presence of the target molecule [46].

Anticoagulant biomaterials with noncovalent cross-linked heparin usually keep heparin working in short time, which is not suitable for use in a flow environment with mechanical shears, especially in blood. The direct covalent graft between heparin and material can provide relatively long-lasting binding of heparin molecules; however, it may also utilize the active sites on heparin molecules and result in loss of its efficiency [50,51]. For example, Alferiev et al. have reported that surface-covalently bound-heparin retains only 11.7% of the activity of free heparin [52].

It was necessary to confirm that the signal trends observed for AT detection on PBMA-Hep and PBMA modified electrode were truly induced by successive AT attachment.

We performed the additions of antithrombin in the PBS solution. Nyquists were obtained with a single electrode for each membrane starting from low to higher concentrations.

A significant difference in the impedance spectra is observed upon the stepwise formation of the complex antithrombin–heparin (ATH). Moreover, by EIS measurement we observed that such self-assembled of the complex is very stable.

For PBMA-Hep the charge transfer resistance increase after adding AT (Table 1) and reaches a saturation value that can be determined with the fitting program. This increase could be attributed to a rearrangement in the structure of heparin when complexed by AT and a variation of the dielectric constant, interpreted by the successful immobilization of AT and saturation of the specific sites. When the film is thick enough, the charge-transfer resistance is mainly influenced by the thickness of polymer film [53].

The incorporation of AT inside the polymer film lead to an increase in the diameter of Nyquist plot. This result proves the insulating character of protein molecules inducing the positive change in charge transfer resistance. AT was therefore successfully embedded within the polymer film.

Fitting results (Tables 1 and 2) show that the film capacitance (C_f), for both PBMA (Table 1) and PBMA-Hep (Table 2), decreases after each addition of AT. These results coincide with the increasing mode of the film thickness relating to Eq. (1):

$$C_f = \frac{\varepsilon \varepsilon_0 A}{df} \quad (1)$$

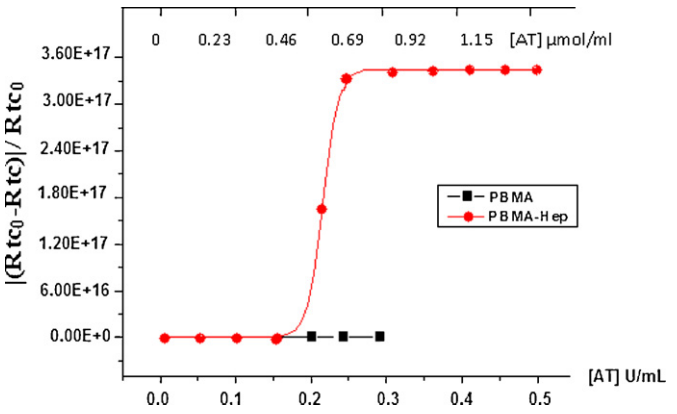

Fig. 7. Calibration plots of the variation of membrane resistance $(\Delta R_m)^N$ with the concentration of ATIII; every point was calculated from measurements of EIS based on the equivalent circuit shown in Fig. 6.

where ε is the dielectric constant of the polymer, ε_0 is the vacuum dielectric constant (8.85×10^{-14} F/cm^2), ε is the dielectric constant of the layer *i* and *A* is the area of the surface, *A* is the electrode area and *df* is the thickness of the polymer layer.

The C_f decreases (Tables 1 and 2) for both polymers coated SS 316L electrode with the addition of the AT, which proves that the layer thickness increases and that AT is directly adsorbed onto the film. AT itself have loops, tails, helixes and sheets that can make their way through the film coated bare metal electrode.

If the sensor is to be used to quantify the analyte concentration and not just to detect its presence, the range of measurable concentrations is important. The dynamic range is the ratio of the largest measurable target concentration and the limit of detection. Dynamic range can be extended on the upper end by simply performing measurements with dilution series of the sample [54].

When the concentration of AT was increased over to 0.2 U/ml and 0.1 U/ml for PBMA-Hep and PBMA respectively, the change of impedance spectra become gradually slow, showing that immobilized AT on the 316L electrode trends to be saturated.

To illustrate the sensitivity of our constructed biosensor, we drawn two plots corresponding to the variation of membrane resistance with AT concentrations.

The values of membrane resistance differences $(\Delta R_m)^N$ (normalized value) vs the added antithrombin concentration were plotted in Fig. 7 for both PBMA-Hep and PBMA films. The change of membrane resistance $(\Delta R_m)^N$ was calculated according to the equation:

$$(\Delta R_m)^N = \frac{|(Rtc_0 - Rtc)|}{Rtc_0} \quad (2)$$

where Rtc_0 is the value of the membrane resistance before AT binding to films coated electrodes and *Rtc* is the value of the membrane resistance after AT binding to films coated electrodes. A linear relationship between the $(\Delta R_m)^N$ values and the concentration of AT was established (Fig. 7).

As it can be seen in Fig. 7, the plot of PBMA-Hep coated electrode is linear for high concentrations of AT and then reaches saturation. This curve shows a linear behavior on a range of concentrations between 0.15 U/ml and 0.25 U/ml then flattens gradually at higher concentrations. This range is close to saturation when the concentration of AT reached 0.3 U/ml.

For PBMA film (Fig. 7), no significant response has been obtained. This behavior allows a low limit detection of AT and indicate no interaction between the AT and the PBMA film.

The linear range of heparin sensor response was achieved at concentration of AT from 0.2 U/ml which corresponds to 0.46 μmol/l while the minimum detectable concentration of AT was 7.35×10^{-7} mol/l on the *in situ* grown nanogold modified sensor [55]. Quantification of bound AT by enzyme immunoassay showed that the concentration of AT binding the heparinized surfaces was 1 μmol/l [56]. Our result shows that the proposed approach is simple and very sensitive compared to the two others.

4. Conclusion

The main objective of this paper was to construct a new kind of anticoagulant biomaterial by copolymerization of heparin with butylmethacrylate.

Interestingly, the obtained copolymer PBMA-Hep formed homogeneous and transparent structures as thin films or discs. Indeed, a peculiar solubility of the copolymer was found in mixtures of THF/H_2O. Physicochemical analysis evidenced intermediate properties between acrylic polymer and heparin.

The possibility of using PBMA-heparin as a coating for the sensor electrode for the study of biomolecules interactions was demonstrated using EIS. Results showed that a PBMA-Hep could be easily deposited on the surface of the sensor electrode for further detecting AT, that the designed biosensor proves high sensitivities and low detection limits (0.46 μmol/l), and demonstrated that AT binding to immobilized heparin is detectable by measuring impedance changes at electrode–solution interfaces with an excellent specificity. Surely, electrochemical impedance spectroscopy showed that the values for the different elements of the equivalent circuit varied according to the layer.

Acknowledgments

We thank Murielle MAIRE, engineer in BPC, for her help with these experiments and for stimulating discussions. We also wish to thank Mme. Virginie GUEGUEN, maître de conferences, of the Department of Chemistry, University Paris 13, for her help with the DSC analyses. The authors gratefully acknowledge Mr Bernard Tribollet and Mr Fernando Pflüger for their help in discussing the results.

References

[1] Z. Yang, J. Wang, R. Luo, M.F. Maitz, F. Jing, H. Sun, N. Huang, Biomaterials 31 (2010) 2072.
[2] J.M. Courtney, N.M. Lamba, S. Sundaram, C.D. Forbes, Biomaterials 15 (1994) 737.
[3] L.O. Andersson, T.W. Barrowcliffe, E. Holmer, E.A. Johnson, G.E.C. Sims, Thromb. Res. 9 (1976) 575.
[4] M. Höök, I. Björk, J. Hopwood, U. Lindahl, FEBS Lett. 66 (1976) 90.
[5] R.D. Rosenberg, P.S. Damus, J. Biol. Chem. 248 (1973) 6490.
[6] I. Björk, T.S. Olson, J.D. Shore, in: D.D. Lane, U. Lindahl (Eds.), Heparin, Chemical, and Biological Properties, Clinical Applications, Edward Arnold, London, 1989, pp. 229–255.
[7] J. Andersson, J. Sanchez, K.N. Ekdahl, G. Elgue, B. Nilsson, R. Larsson, J. Biomed. Mater. Res. 67A (2003) 458.
[8] K. Christensen, R. Larsson, H. Emanuelsson, G. Elgue, A. Larsson, Biomaterials 22 (2001) 349.
[9] R.M. Cornelius, J. Sanchez, P. Olsson, J.L. Brash, J. Biomed. Mater. Res. 67A (2003) 475.
[10] M. Johnell, R. Larsson, A. Siegbahn, Biomaterials 26 (2005) 1731.
[11] R. Kopp, K. Mottaghy, M. Kirschfink, ASAIO J. 48 (2002) 598.
[12] U.R. Nilsson, O. Larm, B. Nilsson, K. Storm, H. Elwing, K.N. Ekdahl, Scand. J. Immunol. 37 (1993) 349.
[13] H. Chen, Y. Chen, H.M.A. Sheardown, Biomaterials 26 (2005) 7418.
[14] D.J. Lin, D.T. Lin, T.H. Young, F.M. Huang, C.C. Chen, L.P. Cheng, J. Membr. Sci. 245 (2004) 137.
[15] B. Meng, X.H. Wang, F.Z. Cui, H.Y. Dong, F. Yu, J. Bioact. Compat. Polym. 19 (2004) 131.
[16] R.M. Cornelius, J. Sanchez, P. Olsson, J.L. Brash, J. Biomed. Mater. Res. A 67A (2003) 475.
[17] J. Laredo, L. Xue, V.A. Husak, J. Ellinger, G. Singh, P.O. Zamora, et al., J. Vasc. Surg. 39 (2004) 1059.
[18] K.D. Park, T. Okano, C. Nojiri, S.W. Kim, J. Biomed. Mater. Res. 22 (1988) 977.
[19] P.F. Hoar, R.M. Wilson, D.T. Mangano, G.J. Avery, R.J. Szarnicki, J.D. Hill, N. Engl. J. Med. 305 (1981) 993.

[20] B. Krafte-Jacobs, C.J. Sivit, R. Mejia, M.M. Pollack, J. Pediatr. 126 (1995) 50.
[21] G. Conn, A.G. Kidane, G. Punshon, R.Y. Kannan, G. Hamilton, A.M. Seifalian, Expert Rev. Mol. Diagn. 3 (2006) 245.
[22] S.R. Nelson, N.M. deSouza, D.J. Allison, Cardiovasc. Intervent. Radiol. 23 (2000) 252.
[23] I. Capila, R.J. Linhardt, Angew. Chem. Int. Ed. 41 (2002) 390.
[24] H. Zhang, R. Zhao, Z. Chen, D.H. Shangguan, G. Liu, Biosens. Bioelectron. 21 (2005) 121.
[25] Z. Qundan, H. Yanyan, Z. Rui, L. Guoquan, C. Yi, J. Colloid Interface Sci. 319 (2008) 94.
[26] J.S. Daniels, N. Pourmand, Electroanalysis 19 (2007) 1239.
[27] O. Panke, T. Balkenhohl, J. Kafka, D. Schafer, F. Lisdat, Adv. Biochem. Eng. Biotechnol. 109 (2008) 195.
[28] S.M. Derkaoui, Revêtement bioactive pour stents métalliques: Synthèse, caractérisation et biocompatibilité, PhD Thesis, Université Paris Nord-Institut Galilée, 2008.
[29] C. Dahlberg, A. Millqvst-Fureby, M. Schuleit, Eur. J. Pharm. Biopharm. 70 (2008) 478.
[30] S. Wu, Polymer Interface and Adhesion, Marcel Dekker, New York, 1982, pp. 25–26 (Chapter 1).
[31] D.L. Schmidt, C.E. Coburn, B.M. DeKoven, G.E. Potter, G.F. Meyers, D.A. Fischer, Nature 368 (1994) 39.
[32] J.L. Feijoo, J.M. Alejandro, J.R. Acosta, J. Mater. Sci. Lett. 5 (1986) 1193.
[33] T. Yang, A. Hussain, S. Bai, I.A. Khalil, H. Harashima, F. Ahsan, J. Control. Release 115 (2006) 289.
[34] R.J. Doyle, Microbes Infect. 2 (2000) 391.
[35] E. Rame, S. Garoff, J. Colloid Interface Sci. 177 (1996) 234.
[36] P. Milleding, S. Gerdes, K. Holmberg, S. Karlsson, Eur. J. Oral Sci. 107 (1999) 384.
[37] D.Y. Kwok, A.W. Neumann, Colloids Surf. A: Physicochem. Eng. Aspects 161 (2000) 31.
[38] C.C. Tsai, Y. Chang, H.W. Sung, J.C. Hsu, C.N. Chen, Biomaterials 22 (2001) 523.
[39] C.O.A. Olsson, D. Landolt, Electrochim. Acta 48 (2003) 1093.
[40] D. Landolt, Corrosion and Surface Chemistry of Metals, CRC Press, Lausanne, 2007.
[41] Y.H. Yau, K. Yang, B. Zhang, Mater. Lett. 61 (2007) 1154.
[42] T. Qinggang, M.A. Barbosaa, C. Fonseca, J. Shen, Biomaterials 24 (2003) 4699.
[43] P. Li, T.C. Tan, J.Y. Lee, Synth. Met. 88 (1997) 237.
[44] T. Tüken, A.T. Özyılmaz, M. Erbil, B. Yazıcı, Proceedings of the Eighth International Corrosion Symposium, Osmangazi University, 2002, p. 194.
[45] M.E. Orazem, N. Pébère, B. Tribollet, J. Electrochem. Soc. 153 (4) (2006) B129–B136.
[46] S.J. Ding, B.W. Chang, C.C. Wu, M.F. Lai, H.C. Chang, Electrochim. Acta 50 (2005) 3660.
[47] F. Mansfeld, M.W. Kendig, in: G.S. Haynes, R. Baboian (Eds.), Laboratory Corrosion Tests and Standards, ASTM STP 866, American Society for Testing and Materials, Philadelphia, PA, 1985, p. 122.
[48] X. Ren, P.G. Pickup, J. Electroanal. Chem. 420 (1997) 251.
[49] R. Ehret, W. Baumann, M. Brischwein, A. Schwinde, K. Stegbauer, B. Wolf, Biosens. Bioelectron. 12 (1997) 29.
[50] S.G. Zhang, D.M. Marini, W. Hwang, S. Santoso, Curr. Opin. Chem. Biol. 6 (2002) 865.
[51] F.J. Spinelli, K.L. Kiick, E.M. Furst, Biomaterials 29 (2008) 1299.
[52] I.S. Alferiev, J.M. Connolly, S.J. Stachelek, A. Ottey, L. Rauova, R.J. Levy, Biomacromolecules 7 (2006) 317.
[53] Q. Ruan, Y. Zhu, F. Lia, J. Xiao, Y. Zeng, F. Xu, J. Colloid Interface Sci. 333 (2009) 725.
[54] J.S. Daniels, N. Pourmand, Label Free Biosensors (2007) 1239 (Review).
[55] Q. Zhang, Y. Huang, R. Zhao, G. Liu, Y. Chen, J. Colloid Interface Sci. 319 (2008) 94.
[56] J.E. Klinth, R.O. Larsson, P.O. Andersson, K. Nilsson Ekdahl, Biosens. Bioelectron. 21 (2006) 1973.